Ultraviolet light-emitting Cd^II complexes: synthesis and property studies

Yuchun Wan, Wei Fan, Yanchao Guo, Cong Chen & Zhenjun Si

⊞ View supplementary material ☐

📅 Accepted author version posted online: 06 Jan 2015.
Published online: 19 Jan 2015.

✎ Submit your article to this journal ☐

📊 Article views: 47

🔍 View related articles ☐

Taylor & Francis
Taylor & Francis Group

Ultraviolet light-emitting CdII complexes: synthesis and property studies

YUCHUN WAN, WEI FAN, YANCHAO GUO, CONG CHEN and ZHENJUN SI*

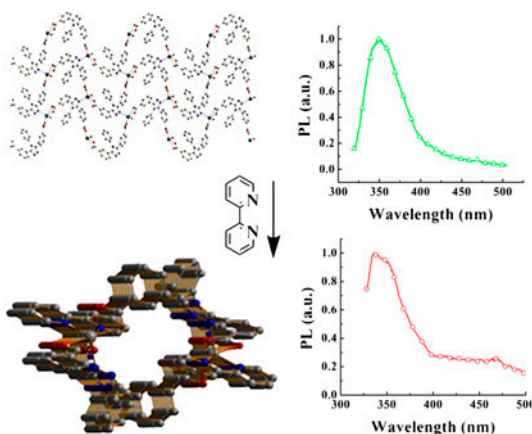School of Materials Science and Engineering, Changchun University of Science & Technology, Changchun, PR China

Four ultraviolet light-emitting CdII complexes were hydrothermally prepared and their single-crystal structures and luminescent properties were fully studied. It is found that the addition of 2,2′-bipyridine not only changes the single-crystal structures, but also the luminescence spectra.

Four ultraviolet light-emitting CdII complexes, $[CdL_1(H_2O)]_n$ (**1**), $[CdL_1(bpy)(H_2O)_2]_n$ (**2**), $[CdL_2(H_2O)]_n$ (**3**), and $[CdL_2(bpy)(H_2O)_2]_n$ (**4**), where L_1 = 3,3′-(4-phenyl-4H-1,2,4-triazole-3,5-diyl)dibenzoate, L_2 = 3,3′-(4-(4-fluorophenyl)-4H-1,2,4triazole-3,5-diyl)dibenzoate, and **bpy** = 2,2′-bipyridine, were hydrothermally synthesized and characterized by single-crystal X-ray diffraction, powder scattering spectra, and infrared spectra. **1**–**4** possess excellent thermal stability with decomposition temperature of *ca.* 340 °C. Their powder samples mainly give luminescent spectra at 350, 339, 351, and 339 nm, respectively, which should be attributed to the ligand-centered $\pi^* \rightarrow \pi$ transfer transitions. Additionally, **1**–**4** have weak emission bands at 400–500 nm, which are tentatively attributed to the triplet ligand to ligand charge transfer transitions.

*Corresponding author. Email: szj@cust.edu.cn

Introduction

Synthesis and property studies of Cd^{II} complexes appealed to a large number of scientific researchers [1–11] because these materials possess catalytic characteristics [4–6] and photophysical properties [7–9]. As a result, organic acids with excellent coordination ability and diverse coordination modes were used to construct Cd^{II} complexes [9, 10]. However, development of luminescent Cd^{II} complexes is still limited, partly due to the fact that Cd^{II} with d^{10} electron configuration, unlike the Re^I, Ir^{III}, and Ru^{III} ions, normally would not present metal complexes with phosphorescent light-emitting properties which could be widely applied in organic light-emitting diodes, optical oxygen detectors, cell labeling, etc. Therefore, exploration of Cd^{II} complexes has been an urgent topic in coordination chemistry [11, 12]. For example, Singh *et al.* reported the influence of the ligand on the structures and luminescent properties of homoleptic Cd^{II} pyridyl functionalized dithiocarbamates [8]. Derivatives of 1,2,4-triazole (**Tz-0**) [13–15], as a nitrogen containing organic compound, were also frequently used in the coordination chemistry [16, 17]. These compounds possess advantages: (i) the nitrogens can coordinate with many metal ions, (ii) the easy modification of **Tz-0** with different functional groups at 3-, 4-, 5-positions gives **Tz-0** derivatives with unexpected properties, and (iii) the large energy gap. Therefore, 3,3′-(4-phenyl-4H-1,2,4-triazole-3,5-diyl)dibenzoic acid (**H₂L₁**) and 3,3′-(4-(4-fluorophenyl)-4H1,2,4-triazole-3,5-diyl)dibenzoic acid (**H₂L₂**) were used in this paper to hydrothermally synthesize four ultraviolet light-emitting Cd^{II} complexes, $[CdL_1(H_2O)]_n$ (**1**), $[CdL_1(bpy)(H_2O)_2]_n$ (**2**), $[CdL_2(H_2O)]_n$ (**3**), and $[CdL_2(bpy)(H_2O)_2]_n$ (**4**), where **bpy** is 2,2′-bipyridine. The molecular structures of **1–4** were verified by infrared (IR) spectroscopy, ultraviolet–visible (UV–vis) absorption spectroscopy, X-ray single-crystal diffraction, and differential thermal analyses. These should be the first examples of ultraviolet light-emitting Cd^{II} complexes.

Results and discussion

Crystal structures

The molecular structures of **1–4** were determined by the X-ray single-crystal diffraction studies. The crystal data of **1–4** are summarized in tables 1 and 2 and the selected molecular parameters are listed in tables S1–S4 (see online supplemental material at http://dx.doi.org/10.1080/00958972.2015.1004055) in the supporting information (SI). X-ray powder diffraction (XRPD) was used to verify the purities of **1–4** and the corresponding XRPD diagrams are presented in figure S1. According to the ORTEP diagram of **1** [figure 1(A)], each Cd^{II} is coordinated in distorted octahedral geometry by three independent L_1^{2-} ligands and a water molecule. The bond lengths of Cd–O (L_1^{2-}) are 2.291–2.451 Å (2.349 Å in average), while the bonds of Cd–N (L_1^{2-}) and Cd–O (water) are 2.264 and 2.231 Å, respectively. Cd^{II} ions array in 1-D S-shape lines along the linkages of L_1^{2-} [figure 1(B)], which extend into 2-D sheets with coordination bonds of Cd–N (L_1^{2-}) [figure 1(C)].

As seen from the ORTEP diagram of **2** [figure 2(A)], each Cd^{II} in **2** is seven-coordinate in distorted decahedral geometry by three independent L_1^{2-} ligands and one **bpy**. The bond lengths of Cd–O (L_1^{2-}) are 2.324–2.523 Å (2.424 Å in average). The bond lengths of Cd–N (**bpy**) are 2.341 or 2.395 Å, while the Cd–N (L_1^{2-}) bond is 2.377 Å. The neighboring Cd^{II} ions in **2** are connected to each other by L_1^{2-} bridges to form the elliptic shape framework [figure 2(B)]. With the help of Cd(01)-N(2) bonds [figure 2(C)], these elliptic frameworks

Table 1. Crystal data and structure refinements for **1** and **2**.

	1	**2**
Empirical formula	$C_{22}H_{13}CdN_3O_5$	$C_{32}H_{25}CdN_5O_6$
M (g M^{-1})	511.75	686.96
Crystal system	Monoclinic	Triclinic
Space group	*Pc*	*P-1*
a (Å)	5.788(5)	9.035(5)
b (Å)	9.276(5)	12.743(5)
c (Å)	18.960(5)	13.372(5)
α (°)	90.000(5)	89.867(5)
β (°)	93.791(5)	71.579(5)
γ (°)	90.000(5)	77.799(5)
V (Å^3)	1015.7(11)	1424.2(11)
Z	2	2
D_{Calcd} (g cm^{-3})	1.673	1.600
$F(0\,0\,0)$	508	692
R_1 $[I > 2\sigma(I)]^a$	0.0410	0.0381
wR_2 (all data)^b	0.1307	0.1125

$^a R_1 = \sum ||F_o| - |F_c|| / \sum |F_o|$.
$^b wR_2 = [\sum w(|F_o| - |F_c|)^2 / \sum w|F_o|^2]^{1/2}$.

Table 2. Crystal data and structure refinements for **3** and **4**.

	3	**4**
Empirical formula	$C_{22}H_{12}CdFN_3O_5$	$C_{32}H_{24}CdFN_5O_6$
M (g M^{-1})	529.75	705.96
Crystal system	Monoclinic	Triclinic
Space group	*Pc*	*P-1*
a (Å)	5.7448(11)	9.0427(11)
b (Å)	9.317(19)	12.8775(16)
c (Å)	18.998(4)	13.5145(16)
α (°)	90.000	89.9540(10)
β (°)	93.14(3)	71.4290(10)
γ (°)	90.000	76.1220(10)
V (Å^3)	1015.3(4)	1443.3(3)
Z	2	2
D_{Calcd} (g cm^{-3})	1.733	1.615
$F(0\,0\,0)$	524	704
R_1 $[I > 2\sigma(I)]^a$	0.0546	0.0270
wR_2 (all data)^b	0.1371	0.0795

$^a R_1 = \sum ||F_o| - |F_c|| / \sum |F_o|$.
$^b wR_2 = [\sum w(|F_o| - |F_c|)^2 / \sum w|F_o|^2]^{1/2}$.

further extend into 1-D tubes [figure 2(D)]. Hence, the **bpy** molecules in **2** lead to a novel single-crystal structure of **2** and prolong the average Cd–O (L_1^{2-}) bond length compared to those in **1**.

Single crystals of **3** (figure S2 in the SI) were prepared when **H₂L₂** was used in the same synthetic procedure for the synthesis of **1**. Cd^{II} ions in **3** possess similar distorted octahedral geometry to those in **1**, with each Cd^{II} ion coordinated by three L_2^{2-} ligands and a water molecule. The lengths of the Cd–O (L_2^{2-}) bonds are 2.286–2.440 Å (2.340 Å in average), while the bond lengths of Cd–O (water) and Cd–N (L_2^{2-}) are 2.239 and 2.258 Å, respectively. Through the contrast of the molecular structures of **1** and **3**, the average Cd–O and Cd–N lengths in **3** are slightly shorter than those in **1**, which should be attributed to the presence of fluorine in L_2^{2-}.
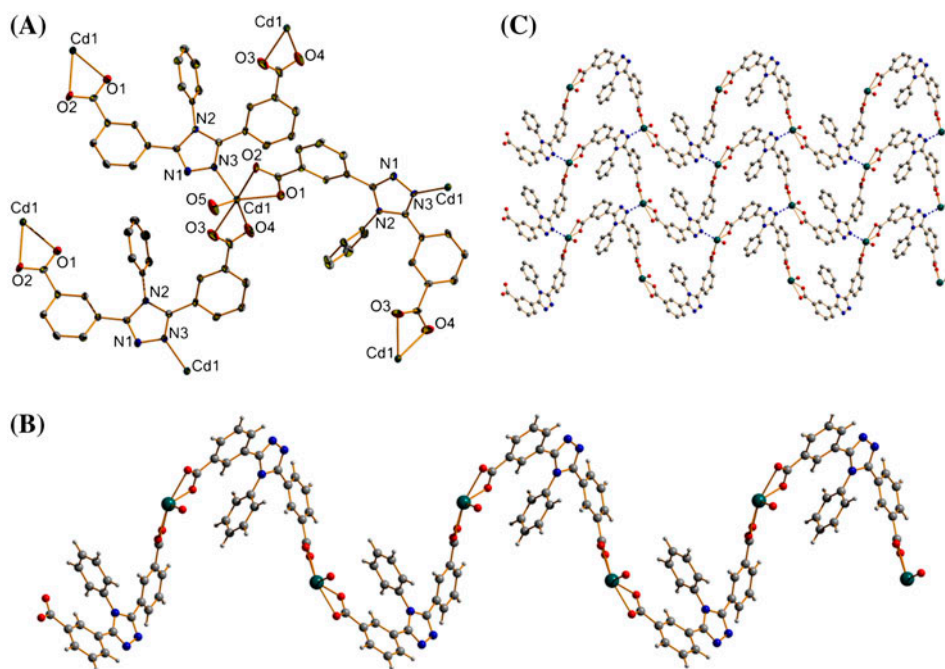
Figure 1. (A) Coordination of **1**. (B) Fragment of 1-D chain of Cd^{II} sustained by the bridge linkages of L_1^{2-} in **1**. (C) Fragment of 2-D sheet in **1**. Hydrogens are not shown for clarity.

To study the effect of the fluorine in **H$_2$L$_2$** and the **bpy** on the molecular structures and photophysical properties (vide infra), crystals of **4** were cultured in similar synthetic procedure for the synthesis of **2**. The molecular structure of **4** is presented in figure S3. Similar to **2**, each Cd^{II} in **4** is seven-coordinate in distorted decahedral geometry by three L_2^{2-} ligands, one **bpy** molecule and one water molecule. The lengths of Cd–O (L_2^{2-}) bonds are 2.306–2.569 Å (2.432 Å in average) and the length of Cd–N (L_2^{2-}) bond is 2.384 Å. The bond lengths of Cd–N (**bpy**) are 2.402 or 2.340 Å. Compared to the molecular structure of **2**, fluorines in L_2^{2-} lead to longer average bond lengths of Cd–O (L_2^{2-}) and Cd–N (L_2^{2-}) in **4**, which is opposite to the effect they had on the molecular structure of **3**. These different effects of fluorine on the single-crystal molecular structures should be mainly attributed to the existence of the coordinated **bpy** in **2** and **4**.

Thermal stability

The thermograms of **1**–**4** are presented in figure 3. The first weight losses between 50–230.0 °C for **1** and **3** were tentatively assigned to the loss of coordination water, while those between 50–130.0 °C for **2** and 50–150.0 °C for **4** should be attributed to the loss of solvent water. These assignments of the weight losses are in agreement with the weight ratios of the water in the corresponding cd^{II} complexes, which are 3.5% for **1**, 5.2% for **2**, 3.4% for **3**, and 5.1% for **4**, respectively. The second decomposition beginning at *ca.* 350.0 °C for **1**, 342.0 °C for **2**, 370.0 °C for **3**, and 336.0 °C for **4**, respectively, should be attributed to the thermal decomposition of the coordinated ligands. These results suggest that **1**–**4** should be stable enough for the common applications.
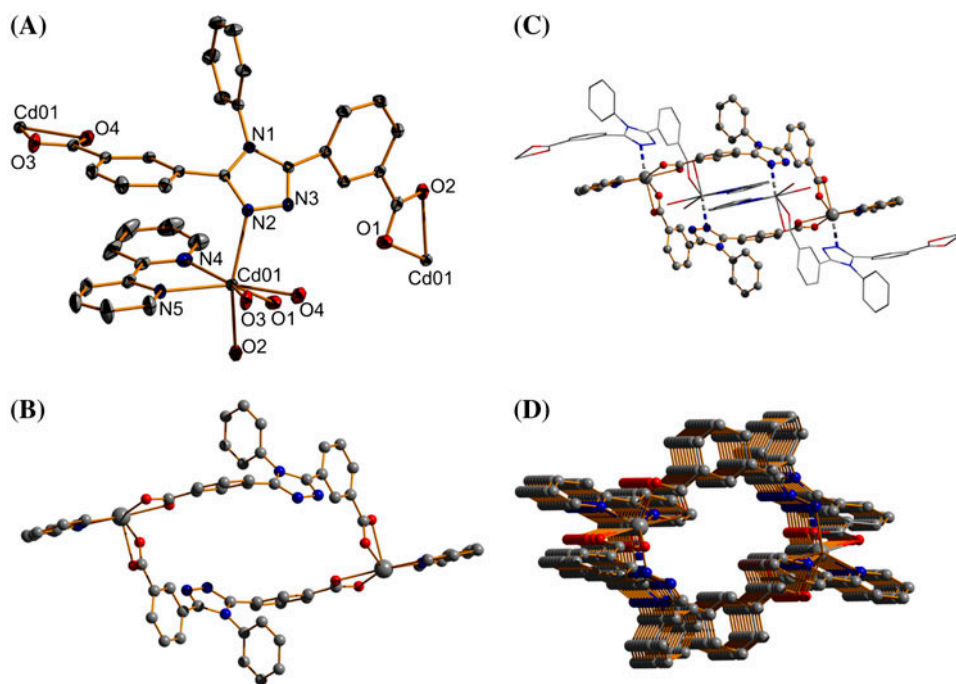
Figure 2. (A) Coordination of **2**. (B) An isolated elliptic shape framework in **2**. (C) Extension between the neighboring elliptic shape frameworks in **2** sustained by the Cd–N bonds. (D) 1-D tube framework in **2**. Hydrogens are not shown for clarity.
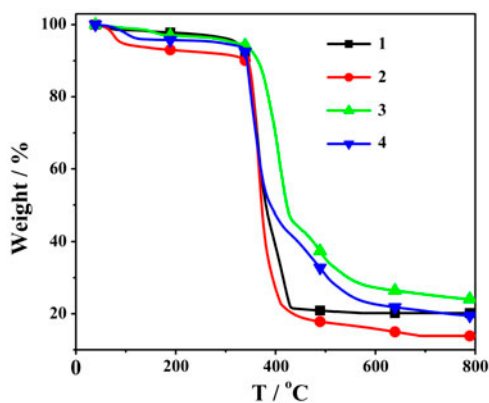

Figure 3. Diagrams of the thermogravimetry analysis for **1**–**4**.

UV–vis absorption properties

The powder scatter spectra of **1**–**4**, along with the UV–vis absorption spectra of **bpy**, **H₂L₁**, and **H₂L₂**, are presented in figure 4. Based on previous reports [18, 19] and the absorption spectra of **bpy**, **H₂L₁**, and **H₂L₂**, the absorption band of **1** centered at *ca.* 230 nm should be
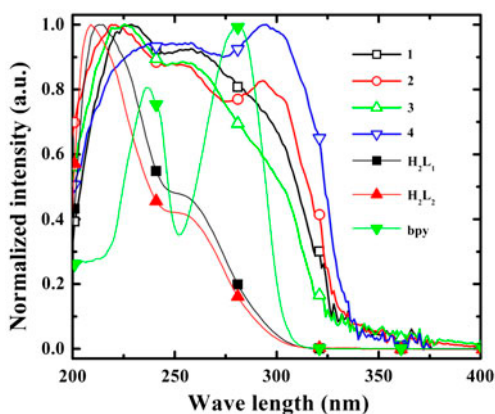
Figure 4. Powder scatter spectra of **1–4** and absorption spectra of **bpy**, H_2L_1, and H_2L_2 measured in the dichloromethane solution (~10^{-5} M/L).

mainly attributed to the $\pi \rightarrow \pi^*$ transitions of L_1^{2-}, while the shoulder band of **1** > 300 nm is tentatively assigned to ligand to ligand charge transfer (LLCT) transitions caused by the Cd^{II} ions. The absorption spectrum of **2** is similar to that of **1** except that the LLCT transitions of **2** are much stronger and split into ^{1}LLCT transitions (~293 nm) and ^{3}LLCT transitions (~304 nm) due to the different coordination modes of Cd^{II} in **1** and **2**. The spectrum of **3** presents blue-shift compared to that of **1** while the spectrum of **4** presents red-shift to that of **2**. These differences should be attributed to the fact that Cd^{II} ions in both **1** and **3** are linked by the bridging ligands (L_1^{2-} or L_2^{2-}) into 1-D S-shaped lines which array in the form similar to the J-aggregation, while the elliptic units in **2** and **4** mainly array in the H-aggregation state. Therefore, fluorine in L_2^{2-} could not only reinforce the dipole of the S-shaped units in **3**, which is in favor of the formation of J-aggregation, but also weaken the dipole of the elliptic units in **4**, which is in favor of the formation of the H-aggregation. According to Tang's research, the J-aggregation and H-aggregation of the molecules would cause the blue-shift and red-shift of the absorption spectra, respectively [20].

Photoluminescent (PL) properties

The solid-state PL spectra of **1–4**, along with those of H_2L_1 and H_2L_2, are recorded at room temperature and presented in figure 5. PL spectra of **1–4** mainly locate in the ultraviolet region (300–400 nm), and the emission bands of **1** (centered at 350 nm) and **2** (centered at 399 nm) are tentatively attributed to the $\pi^* \rightarrow \pi$ transitions of L_1^{2-} based on the PL spectra of H_2L_1 and previously reported results [21]. Similarly, those of **3** (centered at 351 nm) and **4** (centered at 339 nm) should be assigned to the $\pi^* \rightarrow \pi$ transitions of L_2^{2-}. Weak broad emission bands of **2** and **4** extending to 400–500 nm are tentatively attributed to ^{3}LLCT transitions of deprotonated H_2L_1 and H_2L_2, respectively, based on the fact that H_2L_1 and H_2L_2 have similar PL spectra at *ca.* 475 nm at 77 K (figure 5). This assignment is further confirmed by the PL spectra (figure 6) of **1** and **3** measured at 77 K which also present the corresponding weak emission bands at 400–500 nm and are much stronger than those of **2** and **4**.

The $\pi^* \rightarrow \pi$ transition based emission band of **2** (**4**) is almost identical to that of H_2L_1 (H_2L_2), while that of **1** (**3**) is 10 nm red-shift compared to that of H_2L_1 (H_2L_2). These
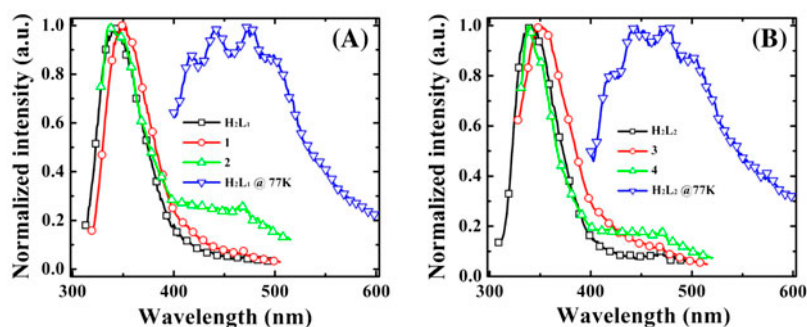
Figure 5.   (A) Solid state emission spectra of H_2L_1, 1 and 2. (B) Solid state emission spectra of H_2L_2, 3 and 4.
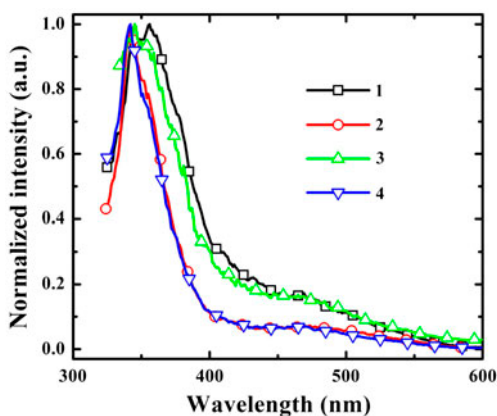

Figure 6.   PL spectra of 1–4 measured at 77 K.

phenomena indicate that **bpy** in **2** (**4**), along with the change of the molecular structures, could partly counteract the effect of narrowing the energy gap between the HOMO and LUMO orbitals caused by coordination between Cd^{II} and L_1^{2-} (L_2^{2-}) in **1** (**3**). This hypothesis is consistent with the fact that the average bond distance of Cd–O in **1**–**4** are **1** (2.349 Å) < **2** (2.424 Å) and **3** (2.340 Å) < **4** (2.432 Å).

Conclusion

Four ultraviolet light-emitting Cd^{II} complexes, **1**–**4**, were synthesized. It was found that **bpy** not only transfer the 2-D sheet-network of **1** and **3** into the 1-D tubes of **2** and **4**, but also leads to longer bond lengths of Cd–O and Cd–N in **2** and **4**. The emission bands of **1**–**4** mainly locate from 300 to 400 nm and could be assigned to ligand-centered $\pi^* \rightarrow \pi$ transitions, and the weaker emission bands of **2** and **4** at 400–500 nm were tentatively assigned to ^{3}LLCT transitions. The effect of fluorine in L_2^{2-} and the coordinated **bpy** on the photophysical properties of **1**–**4** were also studied by the analyses of the UV–vis absorption and PL spectra.

Experimental

All chemicals are used as received without purification. Organic aromatic acids of **H$_2$L$_1$** and **H$_2$L$_2$** were synthesized by previously reported methods [22]. The Cd^{II} complexes were hydrothermally synthesized in poly(tetrafluoroethylene)-lined stainless steel containers under autogenous pressure [23].

Single-crystal structures were measured at 293 K on a Bruker Smart Apex CCD single-crystal diffractometer with λ (Mo Kα) = 0.7107 Å and solved using the SHELXL-97 program [24–26]. The XRPD data were collected on a Panalytical Rigaku Dmax2500 diffractometer with Cu Kα radiation (λ = 1.54056 Å) and step size of 0.02° in the 2θ range of 10°–50°. The IR spectra were acquired on a FTIR-8400S SHIMADZU spectrophotometer from 4000 to 400 cm^{-1}. The powder scatter spectra and the UV–vis absorption spectra were recorded on a Perkin-Elmer Lambda 900 UV/vis/NIR spectrophotometer with a 60 mm Int. Sphere and UVmini-1240 UV–vis spectrophotometer, respectively. The room temperature PL spectra were recorded on a SHIMADZU RF-5301 PC spectrofluorophotometer, while low temperature PL spectra were measured at 77 K with a Lecroy Wave Runner 6100 Digital Oscilloscope (1 GHz) (scan mode) using a tunable laser as the excitation source (Continuum Sunlite OPO). The thermal gravimetric analyses were performed on a Perkin-Elmer thermal analyzer.

Synthesis of [CdL$_1$(H$_2$O)]$_n$ (1)

A mixture of **H$_2$L$_1$** (20.00 mg, 0.05 mM), Cd(NO$_3$)$_2$·4H$_2$O (30.81 mg, 0.10 mM) and distilled water (3 mL) was placed in a 5 mL Teflon liner, then sealed into a stainless steel autoclave and heated at 170 °C for four days to produce colorless block crystals of **1** in 43.0% yield. Anal. Calcd (%) for C$_{22}$H$_{13}$CdN$_3$O$_5$: C, 51.59; H, 2.54; N, 8.21. Found: C, 51.28, H, 2.78, N, 8.35. IR (KBr/cm^{-1}): 3383, 3066, 1611, 1592, 1558, 1499, 1414, 1381, 777, 733, 700.

Synthesis of [CdL$_1$(bpy)(H$_2$O)$_2$]$_n$ (2)

A mixture of **H$_2$L$_1$** (20.00 mg, 0.05 mM), **bpy** (7.5 mg, 0.05 mM), Cd(NO$_3$)$_2$·4H$_2$O (30.81 mg, 0.1 mM), and distilled water (3 mL) was placed in a 5 mL Teflon liner, then sealed into a stainless steel autoclave and heated at 170 °C for four days to produce color-less block crystals of **2** in 48.0% yield. Anal. Calcd (%) for C$_{32}$H$_{25}$CdN$_5$O$_6$: C, 50.14; H, 3.48; N, 19.50. Found: C, 50.20; H, 3.52; N, 19.43. IR (KBr/cm^{-1}): 3466, 3062, 1611, 1594, 1561, 1405, 1391, 783, 776, 700.

Synthesis of [CdL$_2$(H$_2$O)]$_n$ (3)

The synthetic procedure of **3** was similar to that of **1** replacing **H$_2$L$_1$** with **H$_2$L$_2$**, and the colorless block crystals of **3** were synthesized in 51.0% yield. Anal. Calcd (%) for C$_{22}$H$_{12}$CdFN$_3$O$_5$: C, 49.83; H, 2.27; N, 7.93. Found: C, 49.77; H, 2.25; N, 7.99. IR (KBr/cm^{-1}): 3397, 3078, 1611, 1591, 1556, 1511, 1391, 1231, 884, 777, 722.

Synthesis of [CdL$_2$(bpy)(H$_2$O)$_2$]$_n$ (4)

The synthetic procedure of **4** was similar to that of **2** replacing **H$_2$L$_1$** with **H$_2$L$_2$**, and the colorless block crystals of **4** were synthesized in 48.0% yield. Anal. Calcd (%) for C$_{32}$H$_{24}$CdFN$_5$O$_6$: C, 54.39; H, 3.40; N, 9.92. Found: C, 54.38; H, 3.32; N, 9.95. IR (KBr/cm^{-1}): 3469, 3070, 1612, 1594, 1559, 1506, 1405, 1390, 1230, 783, 767, 724.

Supplementary material

The selective bond distances and bond angles, the simulated and measured XRPD patterns, and the crystal structures of **1**–**4**. Crystallographic data for the structural analysis of **1**–**4** have been deposited with the Cambridge Crystallographic Data Center, CCDC 952520–952523, respectively. Copies of this information may be obtained free of the charge from the Director, CCDC, 12 Union Road, Cambridge CB2 1EZ, UK (Fax: +44 1223 336033; E-mail: deposit@ccdc.cam.ac.uk or http://www.ccdc.cam.ac.uk/deposit).

Funding

References

[1] M. Saito, M. Nakajima, S. Hashimoto. *Chem. Commun.*, **36**, 1851 (2000).
[2] V.W.-W. Yam, K.K.-W. Lo. *Chem. Soc. Rev.*, **28**, 323 (1999).
[3] N. Kundu, S.M.T. Abtab, S. Kundu, A. Endo, S.J. Teat, M. Chaudhury. *Inorg. Chem.*, **51**, 2652 (2012).
[4] D.J. Darensbourg, S.A. Niezgoda, J.D. Draper, J.H. Reibenspies. *J. Am. Chem. Soc.*, **120**, 4690 (1998).
[5] S. Adam, A. Bauer, O. Timpe, U. Wild, G. Mestl, W. Bensch, R. Schlögl. *Chem. Eur. J.*, **4**, 1458 (1998).
[6] O. Ohmori, M. Fujita. *Chem. Commun.*, **40**, 1586 (2004).
[7] G.-Y. Wu, Y.-X. Ren, Z. Yin, F. Sun, M.-H. Zeng. *RSC Adv.*, **4**, 24183 (2014).
[8] V. Kumar, V. Singh, A.N. Gupta, K.K. Manar, M.G.B. Drew, N. Singh. *CrystEngComm*, **16**, 6765 (2014).
[9] F. Chen, M.-F. Wu, G.-N. Liu, M.-S. Wang, F.-K. Zheng, C. Yang, Z.-N. Xu, Z.-F. Liu, G.-C. Guo, J.-S. Huang. *Eur. J. Inorg. Chem.*, **2010**, 4982 (2010).
[10] A.J. Calahorro, A. Salinas-Castillo, J.M. Seco, J. Zuñiga, E. Colacio, A. Rodríguez-Diéguez. *CrystEngComm*, **15**, 7636 (2013).
[11] X.-L. Yang, C.-D. Wu. *CrystEngComm*, **16**, 4907 (2014).
[12] A. Moghimi, S. Sheshmani, A. Shokrollahi, H. Aghabozorg, M. Shamsipur, G. Kickelbick, M. Aragoni, V. Lippolis. *Z. Anorg. Allg. Chem.*, **630**, 617 (2004).
[13] J.H. Kim, D.Y. Yoon, J.W. Kim, J.J. Kim. *Synth. Met.*, **157**, 743 (2007).
[14] Z.-L. Zhang, G.-L. Shen, Y. Cheng, Y.-B. Ding, Y.-G. Yin, D. Li. *CrystEngComm*, **12**, 1171 (2010).
[15] J. Li, X. Mi, Y. Wan, Z. Si, H. Sun, Q. Duan, X. He, D. Yan, S. Wan. *J. Lumin.*, **132**, 1200 (2012).
[16] A. Aijaz, E.C. Sañudo, P.K. Bharadwaj. *Cryst. Growth Des.*, **11**, 1122 (2011).
[17] X. Li, B. Wu, R. Wang, H. Zhang, C. Niu, Y. Niu, H. Hou. *Inorg. Chem.*, **49**, 2600 (2010).
[18] W.-T. Chen. *Chin. J. Struct. Chem.*, **32**, 926 (2013).
[19] R.Q. Fan, D.S. Zhu, Y. Mu, G.H. Li, Y.L. Yang, Q. Su, S.H. Feng. *Eur. J. Inorg. Chem.*, **2004**, 4891 (2004).
[20] M. Shimizu, T. Hiyama. *Chem. Asian J.*, **5**, 1516 (2010).
[21] R. Fan, Y. Yang, Y. Yin, W. Hasi, YMu Inorg. *Chem.*, **48**, 6034 (2009).
[22] C.-A. An, Y. Guo, Z. Si, Q. Duan. *J. Fluoresc.*, **24**, 847 (2014).
[23] Y. Guo, T. Shi, Z. Si, Q. Duan, L. Shi. *Inorg. Chem. Commun.*, **34**, 15 (2013).
[24] G.M. Sheldrick. *SHELXTL (Version 5.10)*, Siemens Analytical X-ray Instruments Inc., Madison, WI (1998).
[25] *SMART and SAINT*, Siemens Analytical X-ray Instruments Inc., Madison, WI (1995).
[26] G.M. Sheldrick. *SADABS*, University of Göttingen, Göttingen (1996).